Identification of evolutionary and kinetic drivers of NAD-dependent signalling

Mathias Bockwoldt[1], Dorothée Houry[2], Marc Niere[3], Toni I. Gossmann[4,5], Ines Reinartz[6,7], Alexander Schug[8], Mathias Ziegler[3], and Ines Heiland[1,*]

[1]Department of Arctic and Marine Biology, UiT The Arctic University of Norway, Biologibygget, Framstredet 39, 9017 Tromsø, Norway
[2]Department of Biological Sciences, University of Bergen, Thormøhlens gata 53 A/B, 5006 Bergen, Norway
[3]Department of Biomedicine, University of Bergen, Jonas Lies vei 91, 5009 Bergen, Norway
[4]Department of Animal and Plant Sciences, Western Bank, University of Sheffield, Sheffield, S10 2TN, United Kingdom
[5]Department of Animal Behaviour, Bielefeld University, 33501 Bielefeld, Germany
[6]Department of Physics, Karlsruhe Institute of Technology, Wolfgang-Gaede-Str. 1, 76131 Karlsruhe, Germany
[7]Steinbuch Centre for Computing, Karlsruhe Institute of Technology, Hermann-von-Helmholtz-Platz 1, 76344 Eggenstein-Leopoldshafen, Germany
[8]John von Neumann Institute for Computing, Jülich Supercomputing Centre, Forschungszentrum Jülich, 52425 Jülich, Germany
* Corresponding author: ines.heiland@uit.no

Significance

NAD is best known as essential cofactor of biochemical reactions. In addition, it is involved in the regulation of virtually all major cellular events. These NAD-dependent regulatory functions are mediated by enzymes (e.g. sirtuins, PARPs, ADP-ribosyl cyclases) that cleave the molecule to liberate nicotinamide (Nam). We show that diversification of NAD-dependent signaling in Deuterostomia was accompanied by an optimization of NAD biosynthesis to ensure efficient high affinity recycling of Nam into NAD through Nam-phosphoribosyltransferase (NamPT). In addition, a Nam-methyltransferase (NNMT) emerged which facilitates high NAD-dependent signaling turnover by preventing accumulation of inhibitory Nam. This unexpected kinetic interplay between NamPT and NNMT needs to be considered in therapeutic strategies targeting these enzymes.

Abstract

NAD provides an important link between metabolism and signal transduction and has emerged as central hub between bioenergetics and all major cellular events. NAD-dependent signalling, e.g. by sirtuins and PARPs, consumes considerable amounts of NAD. To maintain physiological functions, NAD consumption and biosynthesis need to be carefully balanced. Using extensive phylogenetic analyses, mathematical modelling of NAD metabolism and experimental verification, we show that the diversification of NAD-dependent signalling in vertebrates depended on three critical evolutionary events: i) the transition of NAD biosynthesis to exclusive usage of nicotinamide phosphoribosyltransferase (NamPT); ii) the occurrence of nicotinamide N-methyltransferase (NNMT), which diverts nicotinamide (Nam) from recycling into NAD, preventing Nam accumulation and inhibition of NAD-dependent signalling reactions and iii) structural adaptation of NamPT, providing an unusually high affinity towards Nam, necessary to maintain NAD levels. Our results reveal an unexpected co-evolution and kinetic interplay between NNMT and NamPT that enables extensive NAD signalling. This has implications for therapeutic strategies of NAD supplementation and the use of NNMT or NamPT inhibitors in disease treatment.

Keywords: NAD-dependent signalling; NAD biosynthesis, nicotinamide N-methyltransferase (NNMT); nicotinamide phosphoribosyltransferase (NamPT); vitamin supplementation; pathway evolution; NAD pathway dynamics; mathematical modelling of NAD metabolism; phylogenetic pathway analysis;

\body

Introduction

NAD metabolism has received increasing attention, as a number of pathological states including neurodegeneration (1), diabetes (2, 3), obesity (4-7), heart diseases (8, 9), muscle dystrophy (10) , renal dysfunction (11) and different types of cancer (12-14) have been associated with changes in this complex network. It has been established that a gradual decline in NAD during ageing is one of the major driving forces of these age-related pathologies (15-18). In addition, NAD metabolism has been identified to be a key regulator for axonal integrity (19-21). It is therefore not surprising that NAD metabolism has emerged as promising pharmacological target for disease treatment (22-25). However, to fully exploit the therapeutic potential of NAD metabolism, the dynamic and functional interplay between the individual NAD pathway components need to be established.

NAD represents one of the most critical links between cellular signal transduction and energy metabolism. Even though it is best known as cofactor for a multitude of redox-reactions, NAD is involved in a number of signalling processes that consume NAD by cleaving NAD^+ to nicotinamide (Nam) and ADP-ribose (14). These NAD-dependent signalling reactions include poly- and mono-ADP-ribosylation (26, 27), sirtuin-mediated protein deacylation (28), and the synthesis of calcium-mobilizing molecules such as cyclic ADP-ribose (29), and participate in the regulation of virtually all cellular activities. The enzymes involved in these processes are sensitive to the available NAD concentration. Therefore, NAD-dependent signalling can act as a transmitter of changes in cellular energy homeostasis, for example, to regulate gene expression or metabolic activity (30).

The significance of NAD-dependent signalling for NAD homeostasis has long been underestimated. It has now become clear that inhibition of NAD biosynthesis leads to a rapid decline of the cellular NAD concentration (13, 31). This observation documents that NAD-dependent signalling reactions consume substantial amounts of NAD. The resulting NAD turnover differs in a cell-type-specific manner. Measurements of cellular NAD half-life have revealed that it can be as short as 15 minutes (32). To maintain the NAD concentration at physiological levels, NAD biosynthesis needs to act at an equally rapid rate. Imbalances in NAD homeostasis have been associated with a number of different diseases. In this context, it is conceivable that several recent studies have demonstrated impressive health benefits of dietary supplementation with intermediates of NAD biosynthesis including, Nam (4), Nam mononucleotide (NMN) (16) and Nam riboside (NR) (2, 6, 17). Apparently, the exploitation of physiologically less active NAD biosynthetic routes, in addition to the use of Nam as precursor (Figure 1), results in increased NAD concentrations that stimulate beneficial NAD-dependent signalling processes, in particular, protein deacetylation by sirtuins (3, 33).

Owing to the continuous release of Nam through NAD-consuming signalling reactions, NAD salvage using Nam as precursor is the most important NAD synthesis pathway. There are two principal pathways that recycle Nam. Vertebrates use a direct two-step pathway starting with the conversion of Nam into the mononucleotide NMN catalysed by Nam phosphoribosyltransferase (NamPT) using phosphoribosyl pyrophosphate (PRPP) as co-substrate. At least in mammals, a nearly complete recycling of Nam by NamPT is achieved by an extraordinarily high substrate affinity to Nam, the K_M being in the low nanomolar range (34). This appears to be mediated by an ATP-dependent phosphorylation of a histidine residue in the catalytic core (35). Despite the importance of its salvage, Nam can also be marked for excretion by methylation. This reaction is catalysed by Nam N-methyltransferase (NNMT). The presence of this enzyme in vertebrates (36) is among the most enigmatic and counterintuitive features of NAD metabolism. While NamPT is seemingly optimised to recycle even the faintest amounts of Nam back into NAD synthesis, NNMT seems to have no metabolic function other than to remove Nam from NAD metabolism. However, since NNMT uses the general methylation source S-adenosylmethionine, it has been suggested that Nam methylation may act as a metabolic methylation sink (37).

In most prokaryotes as well as in plants and fungi, another pathway consisting of four reactions starting with the deamidation of Nam to nicotinic acid (NA) by the Nam deamidase (NADA) is used. (Figure 1).

The three enzymes that act downstream of NADA belong to the Preiss-Handler pathway that also exists in vertebrates. In this pathway NA is converted into the corresponding mononucleotide (NAMN), in a reaction performed by the NA-specific phosphoribosyltransferase NAPRT. The conversion of both mononucleotides, NMN and NAMN, into their corresponding dinucleotides, NAD and NAAD, is catalysed by the Nam/NA adenylyltransferases (NMNATs) that are essential in all organisms (38). The recycling pathway via NA finally requires re-amidation of NAAD by NAD synthase. This final reaction includes an enzyme adenylation step that consumes ATP. Therefore, the Nam recycling by NADA appears to be energetically less efficient than the recycling pathway starting with NamPT.

We and others have shown earlier that the two NAD biosynthesis pathways starting from Nam (Figure 1) coexist in some eukaryotes (36, 39), as well as in some bacterial species (40). Why these pathways coexist in some organisms and over a very long evolutionary time frame and why NADA nevertheless disappeared in vertebrates, is not known. Whether the occurrence of NNMT may have contributed to these evolutionary processes has also remained unexplored.

In the present study, we performed a comprehensive phylogenetic analysis of the NAD pathways using 793 eukaryotic and 7892 prokaryotic genomes. This large scale analysis revealed that there has been an evolutionary transition resulting in the coexistence of NamPT and NNMT in Deuterostomia, while the deamidation pathway, which is dominant in bacteria, became superfluous. Importantly, this selection for NamPT and NNMT was accompanied by a marked increase in the number of NAD-consuming signalling enzymes. Mathematical modelling of the pathway revealed an unexpected positive kinetic role of NNMT for NAD-consuming signalling fluxes, through prevention of accumulation of Nam, the product of NAD-dependent signalling reactions. In addition, our model predicts that NNMT likely exerted an evolutionary pressure on NamPT to develop a high affinity towards its substrate Nam. Indeed, we identified a short sequence insertion in NamPT, which first occurs in Deuterostomia and appears to modulate the affinity of NamPT. Simulating resource competition, we furthermore show that the presence of high affinity NamPT together with NNMT makes the NADA-dependent pathway obsolete, providing a rationale for the evolutionary transition of the pathway in Metazoa.

Taken together, our analyses suggest that the coexistence of NamPT and NNMT has been a prerequisite to enable the evolutionary development of versatile NAD-dependent signalling mechanisms present in vertebrates.

Results

Paradoxical evolutionary correlation between NAD-dependent signalling and precursor metabolism

To understand the functional roles and potential interplay between the three known enzymes that use Nam as substrate (NamPT, NADA and NNMT, Figure 1), we conducted a comprehensive analysis of the phylogenetic distribution of these three enzymes. As shown in Figure 2A, bacteria, fungi, and plants predominantly possess NADA and only a very limited number of species harbour NamPT. In contrast, most Metazoa lost NADA, and rather possess NamPT together with NNMT. NADA and NamPT, the two enzymes that initiate the two different NAD salvage pathways, show a scattered distribution in bacteria. Co-occurrence of these enzymes is rather rare, and has occasionally been found in bacteria (40) and some marine invertebrates (36).

NNMT seems to have arisen *de novo* or diverged rapidly in the most recent common ancestor of Ecdysozoa and Lophotrochozoa (Figure 2B). We were unable to find any indication for the presence of NNMT in fungi or plants (Blastp e-value cutoff 0.1). Interestingly, NA can be methylated to trigonelline in plants and bacteria (41), but the corresponding enzyme has no homology to NNMT or any other enzyme in Metazoa. Nematodes are the only organisms in which we observed a concomitant presence of NADA and NNMT. In Deuterostomia, the only large clade that possesses only NamPT and seems to have lost NNMT are Sauropsida, and among them especially birds. The reason why about half of the sequenced bird genomes do not seem to harbour *NNMT* remains unclear. The distribution of *NNMT* in birds is quite scattered (SI Appendix Figure S1). It is possible that detection of *NNMT* in some bird genomes failed because of their high GC content (42) or because of difficulties in assembling very small chromosomes commonly found in

birds. The absence of *NNMT* might, alternatively, be related to the differences in the excretion systems. In mammals, the product of NNMT, methyl-Nam, is excreted with the urine. There are few metazoan species for which we could not find NamPT or NADA, while NNMT was detected. We assume that this is due to incomplete genomes in the database, as these species are scarce and their distribution appears to be randomly scattered.

In addition to the phylogenetic distribution of the two Nam salvage enzymes NADA and NamPT, we analysed the phylogenetic diversity of enzymes catalysing NAD-dependent signalling reactions. To do so, we used the previously established classification into ten different families of NAD-consuming signalling enzymes (36), including PARP1-3, PARP4, PARP6/8, PARP7/9-15, PARP16, sirtuins, tankyrases, ADPR-cyclases, mono-ADP-ribosyltransferases and t-RNA-phosphotransferases. The detailed list of templates used for the phylogenetic analyses can be found in SI Appendix Table S1. The numbers shown in Figure 2B denote the average number of NAD-dependent signalling enzyme families found in each clade (for a detailed distribution see SI Appendix Table S2). With the exception of Cnidaria and Lophotrochozoa, we noted an average of three to four families in protostomes, whereas most deuterostome species have, on average, more than eight families with an increasing diversification of enzymes within some of these families, especially PARPs (43).

Taken together, we found that NADA is lost in vertebrates, but strongly preserved in most other organisms, despite the higher energetic requirement of this pathway. Moreover, the transition to having both NamPT and NNMT coincides with a considerable diversification of NAD-dependent signalling. This observation seems counter-intuitive, as one would expect that increased NAD-dependent signalling should be compensated by an increased efficiency of substrate (Nam) utilization for NAD biosynthesis. Since NNMT removes Nam from recycling into NAD, it is not obvious how this enzyme could contribute to higher NAD turnover.

Functional properties of NamPT and NNMT have evolved to maximise NAD-dependent signalling

To resolve this apparent contradiction, we turned to modelling approaches permitting to simulate the behaviour of the complex NAD metabolic network under different conditions. We built a dynamic model of NAD metabolism based on ordinary differential equations using previously reported kinetic data (for details, see Methods and Materials and SI Appendix Table S3).

Given the rather limited information about species-specific expression levels of enzymes, we first assumed equal expression of all enzymes, thereby enabling an initial comparison of metabolic features in rather different organisms. Moreover, due to the lack of specific kinetic data from most organisms, we mainly relied on kinetic constants found for human or yeast enzymes. Wherever possible, we included substrate affinities and known product inhibitions as well as inhibition by downstream metabolites, such as the inhibition of NamPT by NAD (34). Finally, the models assumed that cell growth and consecutive cell divisions are a major driving force for NAD biosynthesis, besides NAD-consuming reactions.

First, we addressed the observed phylogenetic correlation between the transition to the co-occurrence of NamPT and NNMT and the increase in the number of NAD-consuming enzymes. We calculated steady state NAD concentrations and NAD consumption fluxes by simulating NAD biosynthesis via NamPT in the presence or absence of NNMT (Figure 3 A and B). Due to the very low turnover number of NamPT (~0.01/s), we used 40-fold higher NamPT levels compared to the other enzymes to achieve free NAD concentrations in the range reported in the literature (44). NAD concentrations can be further increased with higher NamPT levels (see SI Appendix Figure S3A and B). Since NamPT limits the flux, changing NMNAT levels had no effect under the conditions tested (SI Appendix Figure S3 A and B).

Surprisingly, our simulations predict that the presence of NNMT enables higher rather than lower NAD consumption fluxes (Figure 3A), although it diminishes the steady state concentration of NAD (Figure 3B). The decline in NAD concentration can be compensated by a higher expression of NamPT, which also further increases NAD consumption flux (dashed lines in Figure 3A and B). These results indicate a stimulatory role for NNMT solely on the basis of the enzyme kinetics, without having to invoke any

regulatory mechanism (such as signalling events). It turns out that these results can be explained on the basis of the kinetic parameters of NamPT and NAD-consuming enzymes such as Sirtuin 1 (Sirt1). Most NAD-consuming enzymes are inhibited by their product, Nam. Thus, the presence of NNMT enables higher NAD consumption fluxes, by removing excess Nam from the system (SI Appendix Figure S3D and E). At the same time, a high substrate affinity of NamPT ensures the maintenance of a sufficiently high NAD concentration, although the concentration is, as expected, lower than in the system without NNMT. To verify that the release of Nam inhibition is indeed responsible for the increase in NAD consumption flux, we simulated the network with varying K_i values for the NAD consuming reaction. As can be inferred from SI Appendix Figures S3E and F, increasing the K_i for Nam in a system without NNMT mimics the situation when NNMT is included. In contrast, changing the K_i of NamPT for NAD has no effect. That is, decreased NamPT inhibition by lowered NAD concentrations does not cause the flux increase observed in the presence of NNMT. However, if the NAD concentration is strongly reduced, due to high expression of NNMT, the NAD consumption declines again (SI Appendix Figure S3C and D).

Kinetic parameters of NamPT were previously reported for the human enzyme (34) as well as for some bacterial enzymes (45), the latter having a much lower substrate affinity for Nam. We thus simulated the potential effect of NamPT affinity (K_M) on NAD steady state concentration and NAD consumption flux. In the absence of NNMT, a variation of the substrate affinity of NamPT for Nam is predicted to have very little effect on steady state NAD concentration and NAD consumption flux (Figure 3C and D). In the presence of NNMT, however, NAD consumption flux and NAD concentration would rise with increasing affinity of NamPT (Figure 3E and F).

Remarkably, NAD concentration and consumption flux are both considerably affected by cell division rates in a system without NNMT. Our simulations predict a trade-off between sustainable NAD concentration and consumption flux, in the absence of NNMT. In the presence of NNMT, however, NAD consumption rates and concentrations are almost independent of cell division rates. These observations point to a role of NNMT for NAD homeostasis at varying cell division and consumption rates.

Given that a lower affinity of NamPT has been described for the bacterial enzyme (45) where NNMT is not present, we were wondering if the advantage provided by NNMT is dependent on a high affinity of NamPT. In Figures 3G and H we show the direct comparison of simulations assuming different affinities of NamPT, in the presence or absence of NNMT. Interestingly, a low affinity that is in the range of the affinity of NADA for Nam and far above those measured for bacterial NamPTs, leads to higher NAD consumption flux in the presence of NNMT, but only, when cell division rates are low (Figure 3G). However, if the affinity of NamPT is high enough ($K_M << 1$ μM), consumption rates are always higher with NNMT than without. The NAD concentration is, as would be assumed, always lower with NNMT (Figure 3H).

To understand the interplay and competition for Nam between NamPT and NNMT, we conducted simulations in which we scanned a wide range of possible substrate affinities for both enzymes. As shown in Figure 4, these simulations indicate that both NAD consumption flux and NAD concentration would be minimal in case of a low substrate affinity of NamPT and high affinity of NNMT. Conversely, increasing the affinity of NamPT increases NAD consumption, NAD concentration and the flux ratio between NamPT and NNMT reaching a plateau when the substrate affinity of NNMT is sufficiently low. Remarkably, as indicated by the asterisks in Figure 4A, B and C the reported substrate affinities for human NamPT and NNMT (K_M of 5nM and 400 μM, respectively) are within the predicted optimal range, where further adjustment would lead to little or no increase of NAD consumption flux, NAD concentration or NamPT to NNMT flux ratio.

Sequence variance acquired in metazoan NamPT enhances substrate affinity

Given the kinetic interdependence of NNMT and NamPT revealed above, it seemed possible that NNMT exerted an evolutionary pressure on the development of NamPT. In this case, one would expect to observe adaptations that are reflected in the NamPT protein sequence arising in conjunction with the occurrence of NNMT. To explore this, we created a multiple sequence alignment of NamPT protein sequences from Metazoa. An alignment of selected sequences is shown in Figure 5A, a more comprehensive multiple sequence alignment containing a larger number of species can be found in SI Appendix Figure S2. We found an insert of ten amino acids in most Deuterostomia that possess only NamPT and NNMT (indicated

by the blue circle, Figure 5A). This insert corresponds to positions 42 to 51 in the human enzyme and overlaps with a predicted weak nuclear localisation signal (NLS). The NLS prediction is lost when the insert is removed. The ten amino acid insert has so far not been resolved in any of the available crystal structures obtained for NamPT. When modelling this stretch into the known homodimeric structure, the predicted loop, depicted in red in Figure 5B, is connected to one of the β-sheets involved in substrate binding (35). Intriguingly, the loops of the two subunits are in close proximity.

From these observations, we derived two possible hypotheses regarding the role of the loop in NamPT function. The first hypothesis is that the presence of the loop could affect the subcellular localisation of NamPT, as it is overlapping with a predicted NLS. To test this hypothesis, we created a mutant NamPT lacking the loop and recombinantly expressed FLAG-tagged wildtype and mutant NamPT in HeLa S3 cells. Immunofluorescence imaging showed a mixed cytosolic/nuclear localisation for both the wildtype and the mutant NamPT (Figure 5C). Thus, deletion of the loop did not compromise nuclear localisation.

The second hypothesis is based on our model simulations that predict that the presence of NNMT might have exerted evolutionary pressure on NamPT kinetics and that therefore the sequence insertion might have an effect on substrate binding of NamPT. To analyse this possibility, we expressed and purified the wildtype and the mutant enzyme, which lacks the stretch of amino acids 42-51, in *E. coli*, N-terminally fused to a 6xHis-tag. The size exclusion chromatography profile showed that both wildtype and mutant protein were expressed as dimers (see SI Appendix Figure S4C), indicating that the mutant protein was likely folded correctly. The enzymatic activity was assessed by measuring NMN formation. Upon incubation with the NamPT inhibitor FK866 (31) for 30 minutes, neither wildtype nor mutant NamPT did synthesize NMN, suggesting that binding of FK866 is not affected by the mutation (SI Appendix Figure S4D). Using 100 μM Nam and PRPP as substrates, the wildtype showed a turnover rate of 0.0065±0.0010 s^{-1} and 0.0077±0.0006 s^{-1} without and with ATP, respectively, while the mutant did not have any detectable activity (Figure 5D). With 1 mM of both substrates, the turnover rate of the wildtype enzyme increased to 0.0115±0.0005 s^{-1} and 0.0098±0.0010 s^{-1} without and with ATP, respectively. Under these conditions, the turnover rate of the mutant enzyme was 0.0093±0.0008 s^{-1} and 0.0077±0.0006 s^{-1} without and with ATP, respectively. When keeping both PRPP and ATP constant at 1 mM, the wildtype enzyme reaches its maximal rate in the low micromolar range of Nam concentrations (SI Appendix Figure S4E). Under these conditions, activity of the mutant is detectable only at submillimolar Nam concentrations and still rises between 0.5 and 1 mM (SI Appendix Figure S4E) indicating a far lower affinity towards Nam compared to the wildtype. The decrease in activity with ATP at high concentrations of substrates has been observed earlier (34) and has been attributed to the competitive binding of ATP and PRPP (35). Overall, our observations suggest that human NamPT lacking the amino acid stretch 42-51 is catalytically active, retains its dimeric state and sensitivity to FK866. However, it has a lower activity and affinity to Nam. These observations lend support to the conclusion that the acquisition of this loop in the NamPT of higher vertebrates has led to an increased affinity to Nam, as predicted by our metabolic modelling approach.
To see whether we can find a molecular explanation for the reduced affinity of the mutant enzyme, we analysed different available protein structures of NamPT and tested whether the loop insertion could potentially lead to dynamic structural rearrangements. To this end we applied homology modelling (Figure 5B) and molecular dynamics simulations for structures with and without the loop insertion (Figure 5E). We did not observe substantial structural rearrangements and the molecular dynamics simulations showed only limited structural changes upon loop deletion. Rather, we observed a mostly structurally stable catalytic core. This might be based on the fact that all available protein structures of NamPT differ very little even at the catalytic site (between 0.33Å and 0.95Å see SI Appendix Table S4). Some residues close to the catalytic site showed slightly elevated mobilities in the wildtype structure. However, these elevated mobilities were dominated by rare events during the simulation time of 1μs. They therefore do not appear as a robust change of structural dynamics upon loop insertion.

NNMT made NADA obsolete in vertebrates

Finally, we wished to understand whether NADA may have been lost in vertebrates due to kinetic constraints. As shifts in evolutionary selection pressure may result from competition for resources, we built a two-compartment model, based on the pathway model described above. One compartment contains NADA, while the other one contains either NamPT alone or together with NNMT. Both compartments share a limited Nam source (for model details see SI Appendix Table S3). Without NNMT, the

compartment containing NADA shows a higher NAD consumption rate (Figure 6A), and is able to maintain much higher NAD concentrations especially at low cell division rates (Figure 6B). At high cell division rates, steady state concentrations and NAD-consumption rates in both compartments are similar. As bacteria often have relatively high growth rates and a low number of NAD consuming enzymes, this might explain why, at least in some bacteria, both systems may co-exist.

In the presence of NNMT, the NamPT compartment has both higher NAD consumption rates and higher steady state NAD concentrations than the compartment containing NADA (Figure 6C and 6D). This is, however, dependent on the affinity of NamPT for Nam. If the substrate affinity of NamPT is too low, the NADA compartment is able to maintain higher NAD concentrations and consumption flux. As shown in SI Appendix Figure S6, expression of NADA in addition to NNMT and NamPT provides a slight advantage over NADA alone, as long as NamPT has a low affinity. Taken together, the results suggest that the NADA pathway might have helped in the transition to high affinity NamPT, potentially explaining its co-occurrence with NamPT and NNMT in some invertebrates. Eventually, NADA became obsolete upon emergence of a high affinity NamPT. This, in turn, might have been induced by the appearance of NNMT.

Discussion

The present study has revealed fundamental new insights into the evolution and dynamic interplay of the enzymes in NAD metabolism. Our results show that the occurrence of NNMT enabled the enormous diversification of NAD-consuming signalling enzymes in Deuterostomia. NNMT promotes the removal of excessive Nam produced in the signalling reactions. This is necessary to overcome Nam inhibition of the corresponding enzymes. To enable both high NAD turnover and continuous salvage of Nam into NAD, the kinetic parameters of both human NamPT and NNMT have attained values that are in the optimal range predicted through our simulations (Figure 4). Our analyses have identified a stretch of 10 amino acids in the structure of NamPT which contributes to the unusually high substrate affinity of this enzyme in higher vertebrates. While it remains unclear why lower organisms and plants use primarily the Nam salvage pathway through NADA, our analyses demonstrate that the combination of NamPT and NNMT outcompetes this alternative when high turnover of NAD is required for signalling processes. Consequently, NADA has been lost in vertebrates.

The positive effect of NNMT on NAD-consumption flux, especially on sirtuins, is in line with a lifespan extension observed in worms overexpressing NNMT (46). The effect of NNMT overexpression or silencing has been controversially discussed and is presumably tissue and context specific (37). In this regard, it should be noted that, although we predict an overall positive effect of NNMT on NAD consumption rates, excessive expression of NNMT can lead to adverse effects (SI Appendix Figure S3C). Moreover, our analyses predict that the presence of NNMT generally lowers the Nam concentration and reduces cellular NAD concentrations. This effect can, however, be counterbalanced by increased NamPT expression (47, 48). The moderate effects of NNMT expression changes on NAD concentrations (SI Appendix Figure S3D) might explain why some experimental results reported in the literature seem inconsistent. For example, a considerable decrease of liver NAD levels has been reported upon NNMT overexpression (49), while no changes in NAD concentrations could be detected in other studies (5, 50).

It has been shown that MNam excretion is mostly proportional to Nam uptake (51), supporting our findings that NNMT contributes to NAD-pathway homeostasis. As shown in several recent studies, this homeostatic control by NNMT can be circumvented by supplying NR (2, 52-54) which is not a substrate of NNMT. At the cellular level, NNMT is presumably mainly advantageous, when high NAD-consumption rates are required for tissue function, or even more likely, might be important to prevent spatio-temporal accumulation of Nam within cells due to temporally increased NAD-consumption, e.g. PARP activation through DNA-damage.

The main healthy tissues expressing NNMT are the liver and adipose tissues, while no or only little expression of NNMT is observed in most other organs (55). Increased NNMT expression has been found in several types of cancer (56, 57), and might serve to remove Nam produced by increased NAD-dependent signalling. To maintain high NAD concentrations in the tumours, a concomitant increase of NamPT expression is required, which has indeed been described for some cancers (47, 48). It is worth noticing that

NNMT is only advantageous as long as NamPT affinity and activity are sufficiently high. This suggests that certain types of cancers, which express NNMT at a high level, could potentially be more susceptible to inhibitors of NamPT. Several of such inhibitors are currently tested in clinical studies (23, 58). Based on our analyses, it might be reasonable to test patients for NNMT expression in the tumour tissue. Non-NNMT expressing tumours might respond less to competitive NamPT inhibitors, because deficient Nam degradation in those cancer cells would potentially lead to an accumulation of Nam that could outcompete the inhibitor.

Neither the scattered distribution of NamPT and NADA that is especially pronounced in bacteria (40), nor the loss of NADA in the ancestor of vertebrates has been understood earlier. Our combined phylogenetic-modelling analysis provides a potential explanation for both observations. Using simulated competition between two compartments that share the same limited source of Nam, we show that the compartment that contains NamPT and NNMT can maintain a higher steady state NAD concentration and NAD consumption rate than the compartment containing NADA (Figure 6). This is, however, only the case, if NamPT's substrate affinity is sufficiently high. The dominant enzyme combination found in vertebrates, a high-affinity NamPT along with NNMT, thus seems to provide a competitive advantage when high NAD turnover rates are needed. This is not necessarily the case in organisms that use Nam recycling through NADA

In our analyses, we did not consider the potential effects of most co-substrates of the investigated pathway. These co-substrates include targets of the NAD-consuming enzymes, such as acylated proteins for sirtuins, or phosphoribosyl pyrophosphate (PRPP) and ATP required for NMN synthesis by NamPT. However, we did perform an analysis of the effect of concentration changes in the methyl donor *S*-adenosyl methionine (SAM). Its precursor methionine has been shown to potentially limit the effect of NNMT (57). As shown in SI Appendix Figures S3G and H SAM can have both positive and negative effects on the NAD consumption flux, depending on the SAM concentration range. The effects observed in the physiological SAM concentration range (59) are, however, much smaller than those observed for expression changes in NNMT or NamPT (SI Appendix Figure S3C and A respectively). Nevertheless, changes in methionine metabolism, might under some conditions influence cellular NAD concentration and NAD consumption rates. As NNMT in turn consumes SAM, NNMT might not only provide a kinetic advantage for NAD metabolism, but is likely to have a role in regulating other cellular processes through its impact on SAM availability (37). For example, it has been shown that the product MNam can induce the expression of sirtuins (46, 50, 60). However, the underlying mechanisms are still unknown.

In conclusion, we have comprehensively analysed the functional co-evolution of several enzymes of the NAD pathway. The appearance of NNMT apparently initiated and drove complex alterations of the pathway such as an increase and diversification of NAD-dependent signalling, paralleled by an increase in NamPT substrate affinity. Remarkably, when analysing the possibility of co-evolutionary developments within the NAD pathway, we also noted that the loss of NADA and the loop insertion in NamPT co-occurred with the appearance of a human-like NMNAT2 (schematic overview see Figure 7, details SI Appendix Figure S7-S9). Moreover, the occurrence of human-like NMNATs 1 and 3 and thus the further compartmentalisation of NAD metabolism (61) coincided with a site-specific positive selection event in NNMT (see SI Appendix Figure S7 and S8). This might point to a role of NNMT in NAD pathway compartmentalisation in addition to spatio-temporal regulation of the pathway in general.

Methods and Materials

Phylogenetic Analysis

Functionally verified sequences of NNMT, NADA, NamPT, and NAD-consuming enzymes were used as sequence templates for a Blastp analysis against the NCBI non-redundant protein sequence database. For a list of template sequences see SI Appendix Table S1. Blastp parameters were set to yield maximum 20 000 target sequences, using the BLOSUM62 matrix with a word size of 6 and gap opening and extension costs of 11 and 1, respectively. Low-complexity filtering was disabled. To prevent cross-hits, a matrix was created in which the lowest e-values were given at which Blast yielded the same result for each query protein pair. With help of the matrix, the e-value cut-off was set to 1e-30 for all enzymes. To further prevent false positives, a minimal length limit was set based on a histogram of the hit lengths found for each query

protein, excluding peaks much lower than the total protein length. Length limits are given in SI Appendix Table S1. In addition, obvious sequence contaminations were removed by manual inspection of the results. The taxonomy IDs of the species for each enzyme was derived from the accession2taxonomy database provided by NCBI. Scripts for creating, analysing, and visualising the phylogenetic tree were written in Python 3.5, using the ETE3 toolkit (62) and are accessible through the following GitHub repository https://github.com/MolecularBioinformatics/Phylogenetic-analysis.

Dynamic modelling

Kinetic parameters (substrate affinity (K_M) and turnover rates (k_{cat}), substrate and product inhibitions) were retrieved from the enzyme database BRENDA and additionally evaluated by checking the original literature especially with respect to measurement conditions. Parameter values from mammalian species were used if available. For enzymes not present in mammals, values from yeast were integrated. The full list of kinetic parameters including reference to original literature can be found in SI Appendix Table S3. For NMNAT, the previously developed rate law for substrate competition was used (63). Otherwise, Henri-Michaelis-Menten kinetics were applied for all reactions except the import and efflux of Nam, which were simulated using constant flux and mass action kinetics, respectively. Steady state calculation and parameter scan tasks provided by COPASI 4.25 (64) were used for all simulations. The model files are accessible through the Biomodels database accession no. MODEL1905220001 and MODEL1905220002. Related figures were generated using Gnuplot 5.0.

Generation of expression vectors encoding wildtype and mutant human NamPT

For eukaryotic expression with a C-terminal FLAG-epitope, the open reading frame (ORF) encoding human NamPT was inserted into pFLAG-CMV-5a (Merck - Sigma Aldrich) via EcoRI/BamHI sites. Using a PCR approach, this vector provided the basis for the generation of a plasmid encoding a NamPT deletion mutant lacking amino acid residues 42-51 (Δ42-51 NamPT). For prokaryotic expression with an N-terminal 6xHis-tag, the wildtype and mutant ORFs were inserted into pQE-30 (Qiagen) via BamHI and PstI-sites. All cloned sequences were verified by DNA sequence analysis.

Transient transfection, immunocytochemistry, and confocal laser scanning microscopy

HeLa S3 cells cultivated in Ham's F12 medium supplemented with 10% (v/v) FCS, 2 mM L-glutamine, and penicillin/streptomycin, were seeded on cover slips in a 24 well plate. After one day, cells were transfected using Effectene transfection reagent (Qiagen) according to the manufacturer's recommendations. Cells were fixed with 4% paraformaldehyde in PBS 24 hours post transfection, permeabilised (0.5% (v/v) Triton X-100 in PBS) and blocked for one hour with complete culture medium. After overnight incubation with primary FLAG-antibody (mouse M2, Sigma-Aldrich) diluted 1:2500 in complete medium, cells were washed and incubated for one hour with secondary AlexaFluor 594-conjugated goat anti mouse antibody (ThermoFisher, Invitrogen) diluted 1:1000 in complete culture medium. Nuclei were stained with DAPI and the cells were washed. The cover slips were mounted onto microscope slides using ProLong Gold (ThermoFisher, Invitrogen). Confocal laser scanning microscopy of cells was performed at the Molecular Imaging Center at the Department of Biomedicine (University of Bergen), using a Leica TCS SP8 STED 3x microscope equipped with a 100x oil immersion objective (numerical aperture 1.4).

NamPT expression

E. coli BL21-CodonPlus (DE3)-RIL (Agilent) were transformed with pQE-30 NamPT WT or pQE-30 Δ42-51 NamPT along with pREP4 (Qiagen) encoding the lac repressor. Bacterial cells were grown at 37°C in 1 L of Luria-Bertani broth supplemented with 100 µg/mL ampicillin, 50 µg/mL kanamycin and 32 µg/mL chloramphenicol. Protein expression was induced with 0.2 mM isopropyl-β-D-thiogalactoside at 0.4∼0.6 OD_{600}, and cells were subsequently grown overnight at 18 °C.

Purification of NamPT

The cells were harvested by centrifugation and resuspended in lysis buffer (20 mM Tris-HCl pH 8.0, 500 mM NaCl, 4 mM dithiothreitol (DTT), 1 mg/ml lysozyme, 1X Complete EDTA-free protease inhibitor

cocktail (Roche)). After sonication, the lysate was centrifuged at 13,000 g for 30 min. The supernatant was incubated with 2 ml of Nickel-NTA resin (Qiagen). Non-specific protein binding was removed with washing buffer (20 mM Tris-HCl pH 8.0, 500 mM NaCl, 1 mM DTT, 20 mM imidazole). The protein was eluted with 2.5 ml of elution buffer (20 mM Tris-HCl pH 8.0, 500 mM NaCl, 1 mM DTT, 300 mM imidazole).

The eluted protein was immediately subjected to size exclusion chromatography (SEC) using an ÄKTA pure system (GE Healthcare) equipped with a HiLoad 16/60 Superdex 200 pg column (GE Healthcare). The chromatography was performed at a flow rate of 1 ml/min with SEC buffer (20 mM Tris-HCl pH 8.0, 500 mM NaCl). Fractions containing the recombinant protein were pooled and used for enzymatic assays. The purity and size of the protein were assessed by SDS-PAGE.

Enzymatic Assay

In a final volume of 1.2 ml reaction buffer (20 mM Tris-HCl pH 8.0, 500 mM NaCl, 6 mM $MgCl_2$, 0.03% (w/v) BSA), 2 µM of enzyme were incubated with 5-phospho-D-ribose 1-diphosphate (PRPP) and Nam (100 µM or 1 mM both). The reaction was incubated at 30 °C for 10 min and stopped by adding 100 µM of FK866. Subsequently, the samples were frozen in liquid nitrogen. The amount of NMN produced was analysed using NMR spectroscopy. To do so the samples were dried with an Eppendorf Vacufuge Concentrator, and then resuspended in 200 µl of NMR solvent containing 5% (v/v) deuterated H_2O and 1 mM 4,4-dimethyl-4-silapentane-1-sulfonate (DSS).1D ^1H NMR spectra were acquired on a 850 MHz Ascend Bruker spectrometer equipped with 5 mm TCI triple-resonance CryoProbe and a pulse field gradient along the z-axis. The spectra were acquired with the zgesgppe pulse sequence, allowing water suppression using excitation sculpting with gradients and perfect echo. The temperature was kept constant at 300 K. Data were acquired with 2000 scans, 1 s relaxation delay, 1.6 s acquisition time, and contained 65.000 data points with a spectral width of 14 ppm. The spectra phase and baseline were automatically and manually corrected using TopSpin 3.5 software (Bruker Biospin). Quantification of nicotinamide mononucleotide (NMN) was done by the integration of the peak at 9.52 ppm and DSS used as an internal standard. The raw measurement data are accessible using doi: 10.15490/fairdomhub.1.datafile.2942.1
All experiments were conducted at the Norwegian NMR Platform, NNP (grant 226244/F50).

Molecular dynamics simulations

All-atom molecular dynamics simulations were performed with explicit solvent for wildtype and mutant Δ42-51 NamPT (PDB Code: 2H3D (65)). AMBER99SB-ILDN force field (66) was used with the TIP3P water model (67) in GROMACS 5.1.2 (68). The structures were simulated each in a box of water with distance between the solute and the box set to 0.2 nm at a temperature of 300 K for a total time of 1 µs. A time step of 2 fs and the stochastic dynamics integrator were used. For the evaluation of the root mean square fluctuations (RMSF) the first 100 ns of the simulations were omitted.

Identification of human-like NMNATs and test of positive selection in NNMNTs

For the identification of human-like NMNATs we clustered the retrieved sequences using BAli-Phy (69) (SI Appendix Figure S9). Human-like NMNATs 1, 2, and 3 were identified based on the isoform-specific targeting and interaction domains described in (61).
We conducted a test of positive selection for orthologs of human NNMT from 60 vertebrate species. We obtained coding sequences for all species and aligned the respective protein-translated sequences using MUSCLE (70) and prepared codon-based alignments for further processing with PAL2NAL (71). We used codeml from the PAML package (72) to conduct a branch-site model A test of positive selection. The species names and the underlying tree topology for the codeml runs is depicted in SI Appendix Figure S8B. As a null model we assumed neutrality (e.g. diversifying site class with $dN/dS = \omega = 1$) which then was compared to a model with positive selection ($dN/dS = \omega > 1$). Significance between the two models is assessed using a likelihood ratio test assuming that twice the likelihood difference is χ^2 distributed. The critical value is 3.84 at the 5 % level. Additionally, we identify codons with a site-specific signal of positive selection using a Bayes Empirical Bayes (BEB) analysis with a probability > 0.9 (73).

Acknowledgements

We thank the Norwegian Research Council for funding (grant no. 250395/F20). We furthermore thank for the computation time provided through UNINETT Sigma2 – the National Infrastructure for High Performance Computing and Data Storage in Norway. MZ was supported by a grant from the Norwegian Cancer Society (grant no. 673238). IR and AS received support by the Helmholtz Association Initiative and Networking Fund under project number ZT-I-0003. TIG is supported by a Leverhulme Early Career Fellowship (Grant ECF-2015-453) and a NERC grant (NE/N013832/1). The authors thank Heiko Stark for advice with respect to taxonomic classifications.

Author contribution

IH and MZ conceived the study. MB and TG performed the phylogenetic analysis, IH performed the mathematical modelling, DH and MN performed the experiments, IR performed the MD analyses guided by AS. MZ and IH supervised and guided the investigations. All authors analysed data and contributed to the manuscript preparation.

Declaration of interests

The authors declare no competing interest.

References

1. Ljungberg MC*, et al.* (2012) CREB-activity and nmnat2 transcription are down-regulated prior to neurodegeneration, while NMNAT2 over-expression is neuroprotective, in a mouse model of human tauopathy. *Hum Mol Genet* 21(2):251-267.
2. Trammell SA*, et al.* (2016) Nicotinamide Riboside Opposes Type 2 Diabetes and Neuropathy in Mice. *Sci Rep* 6:26933.
3. Yoshino J, Mills KF, Yoon MJ, & Imai S (2011) Nicotinamide mononucleotide, a key NAD(+) intermediate, treats the pathophysiology of diet- and age-induced diabetes in mice. *Cell Metab* 14(4):528-536.
4. Mitchell SJ*, et al.* (2018) Nicotinamide Improves Aspects of Healthspan, but Not Lifespan, in Mice. *Cell Metab* 27(3):667-676 e664.
5. Kraus D*, et al.* (2014) Nicotinamide N-methyltransferase knockdown protects against diet-induced obesity. *Nature* 508(7495):258-262.
6. Canto C*, et al.* (2012) The NAD(+) precursor nicotinamide riboside enhances oxidative metabolism and protects against high-fat diet-induced obesity. *Cell Metab* 15(6):838-847.
7. Kannt A*, et al.* (2018) A small molecule inhibitor of Nicotinamide N-methyltransferase for the treatment of metabolic disorders. *Sci Rep* 8(1):3660.
8. Hsu CP, Oka S, Shao D, Hariharan N, & Sadoshima J (2009) Nicotinamide phosphoribosyltransferase regulates cell survival through NAD+ synthesis in cardiac myocytes. *Circ Res* 105(5):481-491.
9. Diguet N*, et al.* (2018) Nicotinamide Riboside Preserves Cardiac Function in a Mouse Model of Dilated Cardiomyopathy. *Circulation* 137(21):2256-2273.
10. Ryu D*, et al.* (2016) NAD+ repletion improves muscle function in muscular dystrophy and counters global PARylation. *Sci Transl Med* 8(361):361ra139.
11. Poyan Mehr A*, et al.* (2018) De novo NAD(+) biosynthetic impairment in acute kidney injury in humans. *Nat Med* 24(9):1351-1359.
12. Chiarugi A, Dölle C, Felici R, & Ziegler M (2012) The NAD metabolome – A key determinant of cancer cell biology. *Nature Reviews Cancer* 12(11):741--752.
13. Buonvicino D*, et al.* (2018) Identification of the Nicotinamide Salvage Pathway as a New

Toxification Route for Antimetabolites. *Cell Chemical Biology* 25(4):471--482.e477.
14. Verdin E (2015) NAD+ in aging, metabolism, and neurodegeneration. *Science* 350(6265).
15. Chini CCS, Tarrago MG, & Chini EN (2017) NAD and the aging process: Role in life, death and everything in between. *Mol Cell Endocrinol* 455:62-74.
16. Mills KF*, et al.* (2016) Long-Term Administration of Nicotinamide Mononucleotide Mitigates Age-Associated Physiological Decline in Mice. *Cell Metab* 24(6):795-806.
17. Zhang H*, et al.* (2016) NAD(+) repletion improves mitochondrial and stem cell function and enhances life span in mice. *Science* 352(6292):1436-1443.
18. Imai SI & Guarente L (2016) It takes two to tango: NAD(+) and sirtuins in aging/longevity control. *NPJ Aging Mech Dis* 2:16017.
19. Araki T, Sasaki Y, & Milbrandt J (2004) Increased nuclear NAD biosynthesis and SIRT1 activation prevent axonal degeneration. *Science* 305(5686):1010-1013.
20. Beirowski B*, et al.* (2009) Non-nuclear Wld(S) determines its neuroprotective efficacy for axons and synapses in vivo. *J Neurosci* 29(3):653-668.
21. Di Stefano M*, et al.* (2017) NMN Deamidase Delays Wallerian Degeneration and Rescues Axonal Defects Caused by NMNAT2 Deficiency In Vivo. *Curr Biol* 27(6):784-794.
22. Yoshino J, Baur JA, & Imai SI (2018) NAD(+) Intermediates: The Biology and Therapeutic Potential of NMN and NR. *Cell Metab* 27(3):513-528.
23. Espindola-Netto JM*, et al.* (2017) Preclinical efficacy of the novel competitive NAMPT inhibitor STF -118804 in pancreatic cancer. *Oncotarget* 8(49):85054--85067.
24. Rajman L, Chwalek K, & Sinclair DA (2018) Therapeutic Potential of NAD-Boosting Molecules: The In Vivo Evidence. *Cell Metab* 27(3):529-547.
25. Sinclair DA & Guarente L (2014) Small-molecule allosteric activators of sirtuins. *Annu Rev Pharmacol Toxicol* 54:363-380.
26. Gupte R, Liu Z, & Kraus WL (2017) PARPs and ADP-ribosylation: recent advances linking molecular functions to biological outcomes. *Genes Dev* 31(2):101-126.
27. Bütepage M, Eckei L, Verheugd P, & Lüscher B (2015) Intracellular Mono- ADP -Ribosylation in Signaling and Disease. *Cells* 4(4):569--595.
28. Osborne B, Bentley NL, Montgomery MK, & Turner N (2016) The role of mitochondrial sirtuins in health and disease. *Free Radical Biology and Medicine* 100:164--174.
29. Lee HC (2012) Cyclic ADP -ribose and nicotinic acid adenine dinucleotide phosphate (NAADP) as messengers for calcium mobilization. *Journal of Biological Chemistry* 287(38):31633--31640.
30. Koch-Nolte F, Haag F, Guse AH, Lund F, & Ziegler M (2009) Emerging roles of NAD+ and its metabolites in cell signaling. *Science Signaling* 2(57):mr1.
31. Hasmann M & Schemainda I (2003) FK866, a highly specific noncompetitive inhibitor of nicotinamide phosphoribosyltransferase, represents a novel mechanism for induction of tumor cell apoptosis. *Cancer Res* 63(21):7436-7442.
32. Liu L*, et al.* (2018) Quantitative Analysis of NAD Synthesis-Breakdown Fluxes. *Cell Metabolism* 27(5):1067--1080.e1065.
33. North BJ & Verdin E (2004) Sirtuins: Sir2 -related NAD -dependent protein deacetylases. *Genome Biology* 5(5):224.
34. Burgos ES & Schramm VL (2008) Weak coupling of ATP hydrolysis to the chemical equilibrium of human nicotinamide phosphoribosyltransferase. *Biochemistry* 47(42):11086--11096.
35. Burgos ES, Ho M-C, Almo SC, & Schramm VL (2009) A phosphoenzyme mimic, overlapping catalytic sites and reaction coordinate motion for human NAMPT . *Proceedings of the National Academy of Sciences* 106(33):13748--13753.
36. Gossmann TI*, et al.* (2012) NAD+ biosynthesis and salvage – a phylogenetic perspective. *The FEBS Journal* 279(18):3355--3363.
37. Pissios P (2017) Nicotinamide N -Methyltransferase: More Than a Vitamin B3 Clearance Enzyme. *Trends in Endocrinology and Metabolism* 28(5):340--353.
38. de Figueiredo LF, Gossmann TI, Ziegler M, & Schuster S (2011) Pathway analysis of NAD+ metabolism. *Biochemical Journal* 439(2):341--348.
39. Carneiro J*, et al.* (2013) The Evolutionary Portrait of Metazoan NAD Salvage. *PLoS ONE* 8(5).
40. Gazzaniga F, Stebbins R, Chang SZ, McPeek MA, & Brenner C (2009) Microbial NAD metabolism: lessons from comparative genomics. *Microbiology and Molecular Biology Reviews* 73(3):529--541.

41. Perchat N, *et al.* (2018) Elucidation of the trigonelline degradation pathway reveals previously undescribed enzymes and metabolites. *Proc Natl Acad Sci U S A* 115(19):E4358-E4367.
42. Hron T, Pajer P, Pačes J, Bartůněk P, & Elleder D (2015) Hidden genes in birds. *Genome Biology* 16(1):4--7.
43. Gossmann TI & Ziegler M (2014) Sequence divergence and diversity suggests ongoing functional diversification of vertebrate NAD metabolism. *DNA Repair* 23:39--48.
44. Cambronne XA, *et al.* (2016) Biosensor reveals multiple sources for mitochondrial NAD(+). *Science* 352(6292):1474-1477.
45. Sorci L & Blaby Ia (2010) Genomics-driven reconstruction of \spec Acinetobacter NAD metabolism: Insights for antibacterial target selection. *Journal of Biological Chemistry* 285(50):39490--39499.
46. Schmeisser K, *et al.* (2013) Role of sirtuins in lifespan regulation is linked to methylation of nicotinamide. *Nature Chemical Biology* 9(11):693--700.
47. Bi TQ, *et al.* (2011) Overexpression of Nampt in gastric cancer and chemopotentiating effects of the Nampt inhibitor FK866 in combination with fluorouracil. *Oncology Reports* 26(5):1251--1257.
48. Wang B, *et al.* (2011) NAMPT overexpression in prostate cancer and its contribution to tumor cell survival and stress response. *Oncogene* 30(8):907--921.
49. Komatsu M, *et al.* (2018) NNMT activation can contribute to the development of fatty liver disease by modulating the NAD (+) metabolism. *Sci Rep* 8(1):8637.
50. Hong S, *et al.* (2015) Nicotinamide N -methyltransferase regulates hepatic nutrient metabolism through Sirt1 protein stabilization. *Nature Medicine* 21(8):887--894.
51. Kang-Lee YA, *et al.* (1983) Metabolic effects of nicotinamide administration in rats. *J Nutr* 113(2):215-221.
52. Gong B, *et al.* (2013) Nicotinamide riboside restores cognition through an upregulation of proliferator-activated receptor-gamma coactivator 1alpha regulated beta-secretase 1 degradation and mitochondrial gene expression in Alzheimer's mouse models. *Neurobiol Aging* 34(6):1581-1588.
53. Liu HW, *et al.* (2018) Pharmacological bypass of NAD(+) salvage pathway protects neurons from chemotherapy-induced degeneration. *Proc Natl Acad Sci U S A*.
54. Martens CR, *et al.* (2018) Chronic nicotinamide riboside supplementation is well-tolerated and elevates NAD(+) in healthy middle-aged and older adults. *Nat Commun* 9(1):1286.
55. Aksoy S, Szumlanski CL, & Weinshilboum RM (1994) Human liver nicotinamide N-methyltransferase. cDNA cloning, expression, and biochemical characterization. *Journal of Biological Chemistry* 269(20):14835--14840.
56. Okamura A, *et al.* (1998) Increased hepatic nicotinamide N -methyltransferase activity as a marker of cancer cachexia in mice bearing colon 26 adenocarcinoma. *Japanese Journal of Cancer Research* 89(6):649--656.
57. Ulanovskaya OA, Zuhl AM, & Cravatt BF (2013) NNMT promotes epigenetic remodeling in cancer by creating a metabolic methylation sink. *Nature Chemical Biology* 9(5):300--306.
58. Xu T-Y, *et al.* (2015) Discovery and characterization of novel small-molecule inhibitors targeting nicotinamide phosphoribosyltransferase. *Scientific Reports* 5(1):10043.
59. Reed MC, Nijhout HF, Sparks R, & Ulrich CM (2004) A mathematical model of the methionine cycle. *J Theor Biol* 226(1):33-43.
60. Liu KY, *et al.* (2015) Nicotinamide N-methyltransferase increases complex I activity in SH-SY5Y cells via sirtuin 3. *Biochem Biophys Res Commun* 467(3):491-496.
61. Lau C, *et al.* (2010) Isoform-specific targeting and interaction domains in human nicotinamide mononucleotide adenylyltransferases. *J Biol Chem* 285(24):18868-18876.
62. Huerta-Cepas J, Serra F, & Bork P (2016) ETE 3: Reconstruction, Analysis, and Visualization of Phylogenomic Data. *Molecular Biology and Evolution* 33(6):1635--1638.
63. Schäuble S, Stavrum A-K, Puntervoll P, Schuster S, & Heiland I (2013) Effect of substrate competition in kinetic models of metabolic networks. *FEBS Letters* 587(17):2818--2824.
64. Hoops S, *et al.* (2006) COPASI – a COmplex PAthway SImulator. *Bioinformatics* 22(24):3067--3074.
65. Wang T, *et al.* (2006) Structure of Nampt/PBEF/visfatin , a mammalian NAD+ biosynthetic enzyme. *Nature Structural and Molecular Biology* 13(7):661--662.
66. Lindorff-Larsen K, *et al.* (2010) Improved side-chain torsion potentials for the Amber ff99SB

protein force field. *Proteins* 78(8):1950-1958.
67. Jorgensen WL, Chandrasekhar J, Madura JD, Impey RW, & Klein ML (1983) Comparison of simple potential functions for simulating liquid water. *The Journal of Chemical Physics* 79(2):926--935.
68. Abraham MJ*, et al.* (2015) GROMACS: High performance molecular simulations through multi-level parallelism from laptops to supercomputers. *SoftwareX* 1-2:19--25.
69. Suchard MA & Redelings BD (2006) BAli-Phy: simultaneous Bayesian inference of alignment and phylogeny. *Bioinformatics* 22(16):2047-2048.
70. Edgar RC (2004) MUSCLE: a multiple sequence alignment method with reduced time and space complexity. *BMC Bioinformatics* 5:113.
71. Suyama M, Torrents D, & Bork P (2006) PAL2NAL: robust conversion of protein sequence alignments into the corresponding codon alignments. *Nucleic Acids Res* 34(Web Server issue):W609-612.
72. Yang Z (2007) PAML 4: phylogenetic analysis by maximum likelihood. *Mol Biol Evol* 24(8):1586-1591.
73. Yang Z, Wong WS, & Nielsen R (2005) Bayes empirical bayes inference of amino acid sites under positive selection. *Mol Biol Evol* 22(4):1107-1118.
74. Arnold K, Bordoli L, Kopp J, & Schwede T (2006) The SWISS-MODEL workspace: A web-based environment for protein structure homology modelling. *Bioinformatics* 22(2):195--201.
75. Biasini M*, et al.* (2014) SWISS-MODEL : Modelling protein tertiary and quaternary structure using evolutionary information. *Nucleic Acids Research* 42(W1):252--258.
76. Anonymous (2007) Tree of Life Web Project. eds Maddison DR & Schulz K-S.

Figure Legends

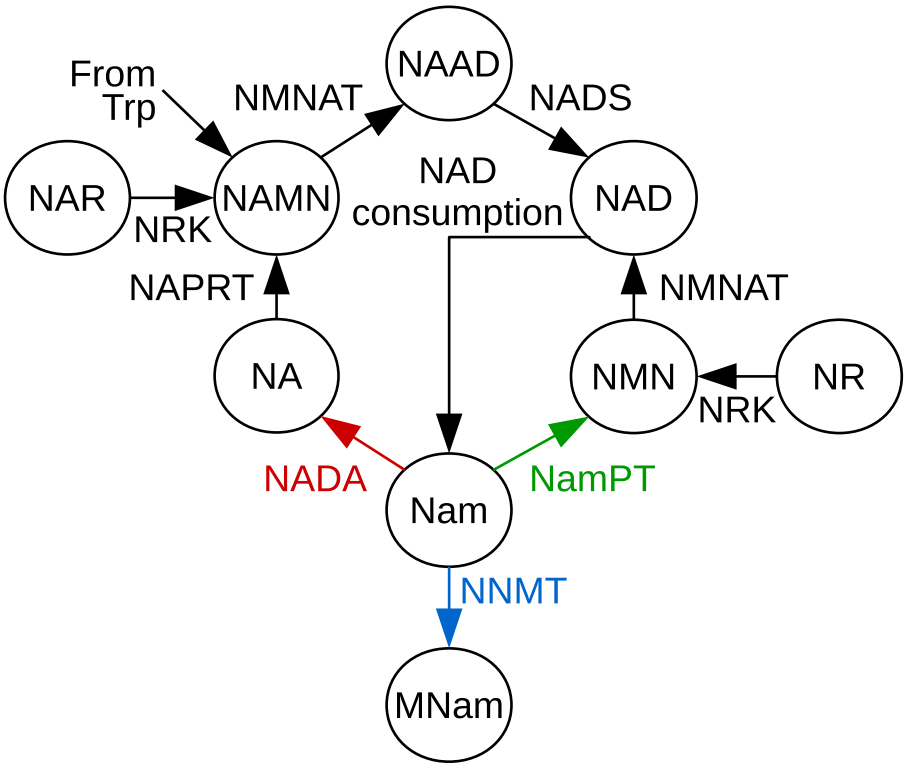

Figure 1: Schematic overview of NAD biosynthesis pathways. NAD can be synthesised from tryptophan (Trp), nicotinamide (Nam), nicotinic acid (NA) and the corresponding ribosides NR and NAR. Nam is the main precursor in humans and also the product of NAD-consuming signalling reactions by enzymes such as sirtuins (NAD-dependent deacylases) or PARPs (poly-ADP-ribose polymerases). For the recycling of Nam, two different pathways exist. The pathway found in yeast, plants, and many bacteria starts with the deamidation of Nam by Nam deamidase (NADA). Further biosynthesis via the Preiss-Handler pathway, which also exists in vertebrates, requires three subsequent enzymatic steps catalysed by Nicotinic acid phosphoribosyltransferase (NAPRT), Nicotinic acid/Nicotinamide mononucleotide adenylyltransferase (NMNAT) and NAD synthase (NADS). In vertebrates, Nam is directly converted to nicotinamide mononucleotide (NMN) by Nam phosphoribosyltransferase (NamPT). The Nam N-methyltransferase

(NNMT) degrades Nam to methyl-Nam (MNam), which, in mammals, is excreted with the urine. The colour code for the three different enzymes utilizing Nam is used in subsequent figures to denote the presence of these enzymes in different organisms.

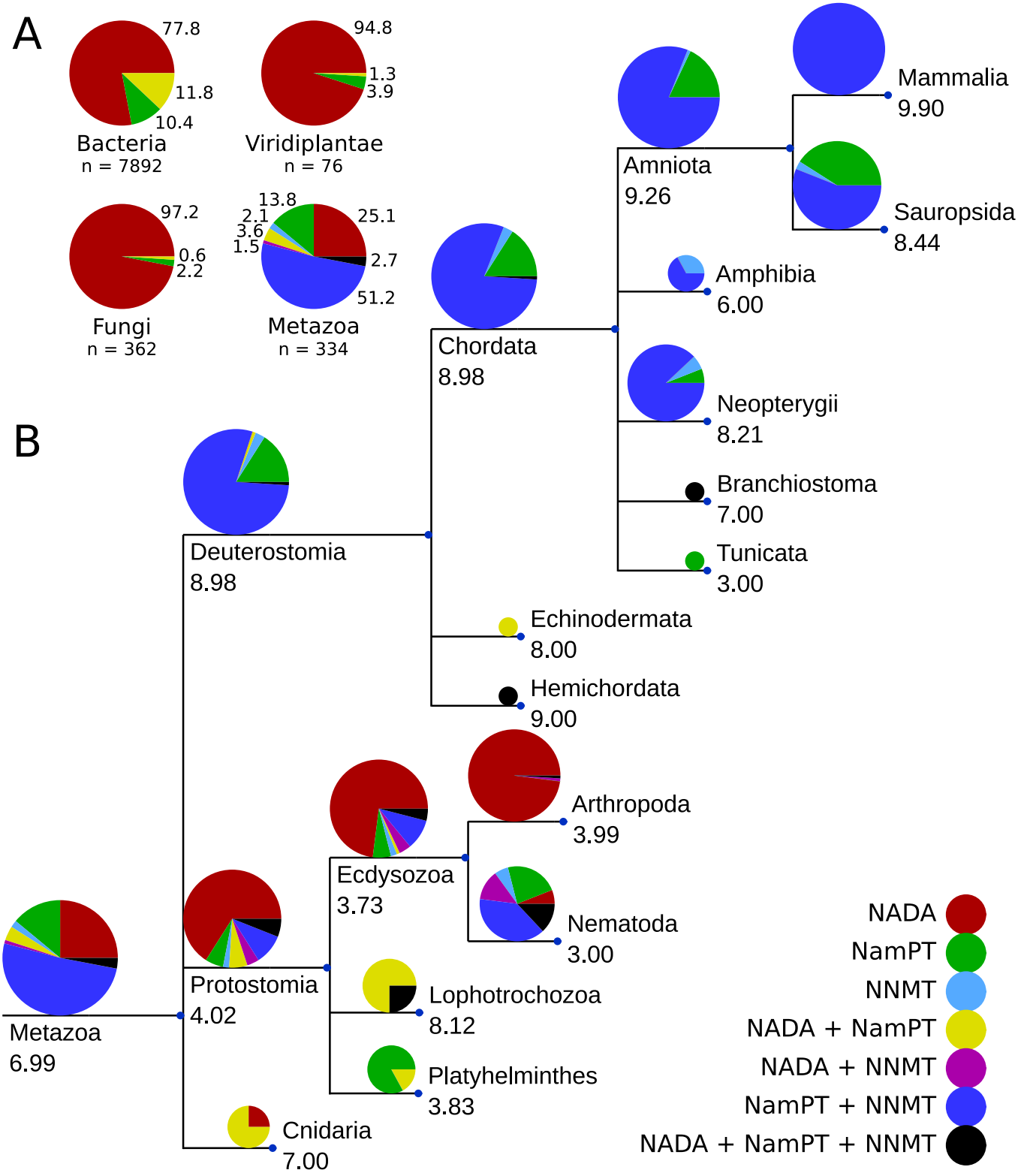

Figure 2: Phylogenetic distribution of NADA, NNMT, and NamPT and their relation to the number of NAD consumers. A) Distribution of NADA, NNMT, and NamPT in selected clades. NADA is dominant in bacteria, fungi, and plants (Viridiplantae), whereas NamPT together with NNMT is dominant in Metazoa. Numbers at the pie charts show the percentage of species per clade, which possess the respective enzyme combination indicated by the colour code explained in the lower right of the figure (n = number of species per clade included in the analysis). **B)** Common tree of selected clades within Metazoa, including 334 species. The pie charts indicate the distribution of species within the respective clade that encode the enzyme combination indicated by the different colours. The size of the pie charts is proportional to the logarithm of the number of species analysed in the particular clade. The numbers below the clade names

indicate the average number of NAD-consuming enzyme families found in all species of that clade. The branch length is arbitrary. A detailed analysis of birds is provided in SI Appendix Figure S1 and the template sequences used for the analysis are listed in SI Appendix Table S1.

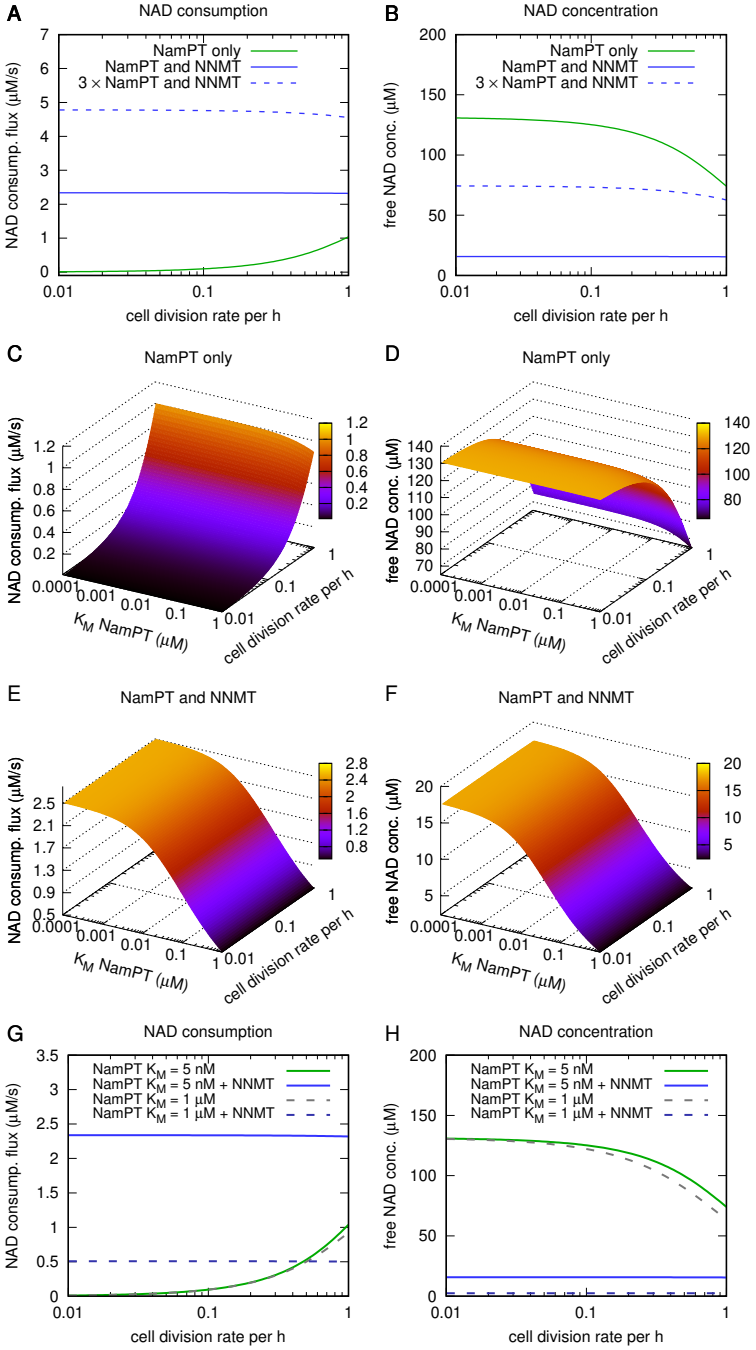

Figure 3: NNMT enables high NAD consumption flux and is a potential driver of NamPT affinity increase. A dynamic model of NAD biosynthesis and consumption (for details, see Methods and Materials and SI Appendix Table S3) was used to simulate **A)** steady state NAD consumption flux and **B)** NAD concentration. Except for the results shown as dashed line in A and B, the enzyme amounts were kept constant for all simulations shown. In the presence of NNMT (blue curves), steady state NAD consumption rates are higher despite reduced NAD concentrations. Increasing the amount of NamPT in the simulation threefold (dotted blue curves) partially compensates for the decreased NAD concentration caused by Nam degradation through NNMT. The potential effect of different affinities of NamPT for Nam (inversely proportional to the Michaelis-Menten constant, K_M) on the steady state NAD consumption flux and NAD concentration was simulated at different cell division rates. In the absence of NNMT, the affinity of NamPT has little influence on **C)** NAD consumption and **D)** NAD concentration, but both are strongly influenced by cell division rates. **E and F)** in the presence of NNMT, increasing affinity of NamPT enables increasing NAD consumption flux and NAD concentration. The presence of NNMT makes both NAD consumption flux and concentration almost independent of cell division rates. **G and H)** calculated NAD consumption

fluxes and free NAD concentrations, respectively, are shown for the assumption of high affinity of NamPT (K_M = 5 nM, as found in the human enzyme) and low affinity (1 µM, dashed lines). Comparing the situation with and without NNMT reveals that, at low substrate affinity of NamPT and high cell division rates, NNMT no longer enables higher NAD consumption rates compared to NamPT alone (green curves and dashed grey curves).

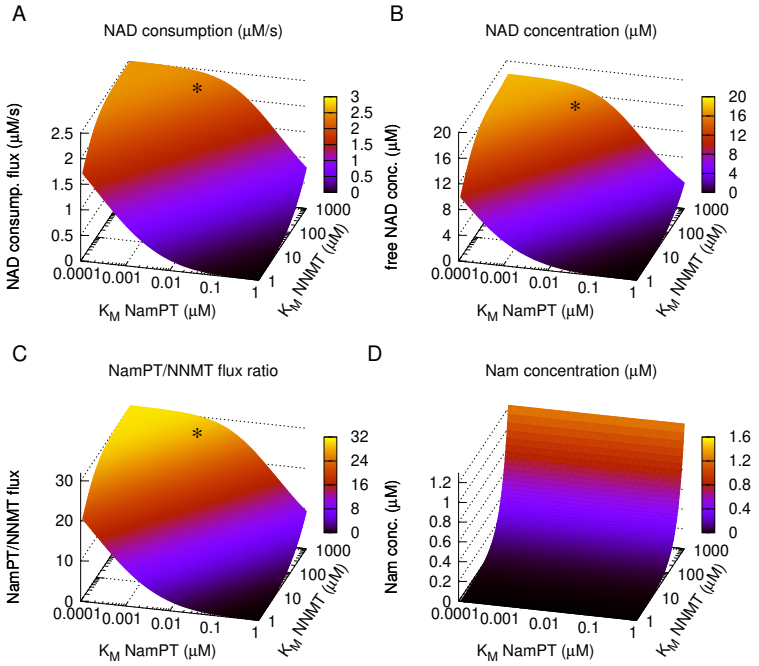

Figure 4: Evolutionary optimality of the substrate affinities of human NNMT and NamPT. We simulated the impact of changes in the substrate affinities of both NamPT and NNMT on **A)** NAD consumption rates, **B)** free NAD concentration, **C)** NamPT/NNMT flux ratio and **D)** Nam concentration. With increasing affinity of NamPT (decreasing K_M), but decreasing *affinity* of NNMT (increasing K_M) NAD consumption rates and free NAD concentrations as well as the ratio between NamPT and NNMT flux are augmented. The affinities reported for human enzymes (indicated by a black asterisk) appear to be in the optimal range according to our simulations. The steady state concentration of Nam is largely independent of the substrate affinity of NamPT, but strongly dependent on the affinity of NNMT.

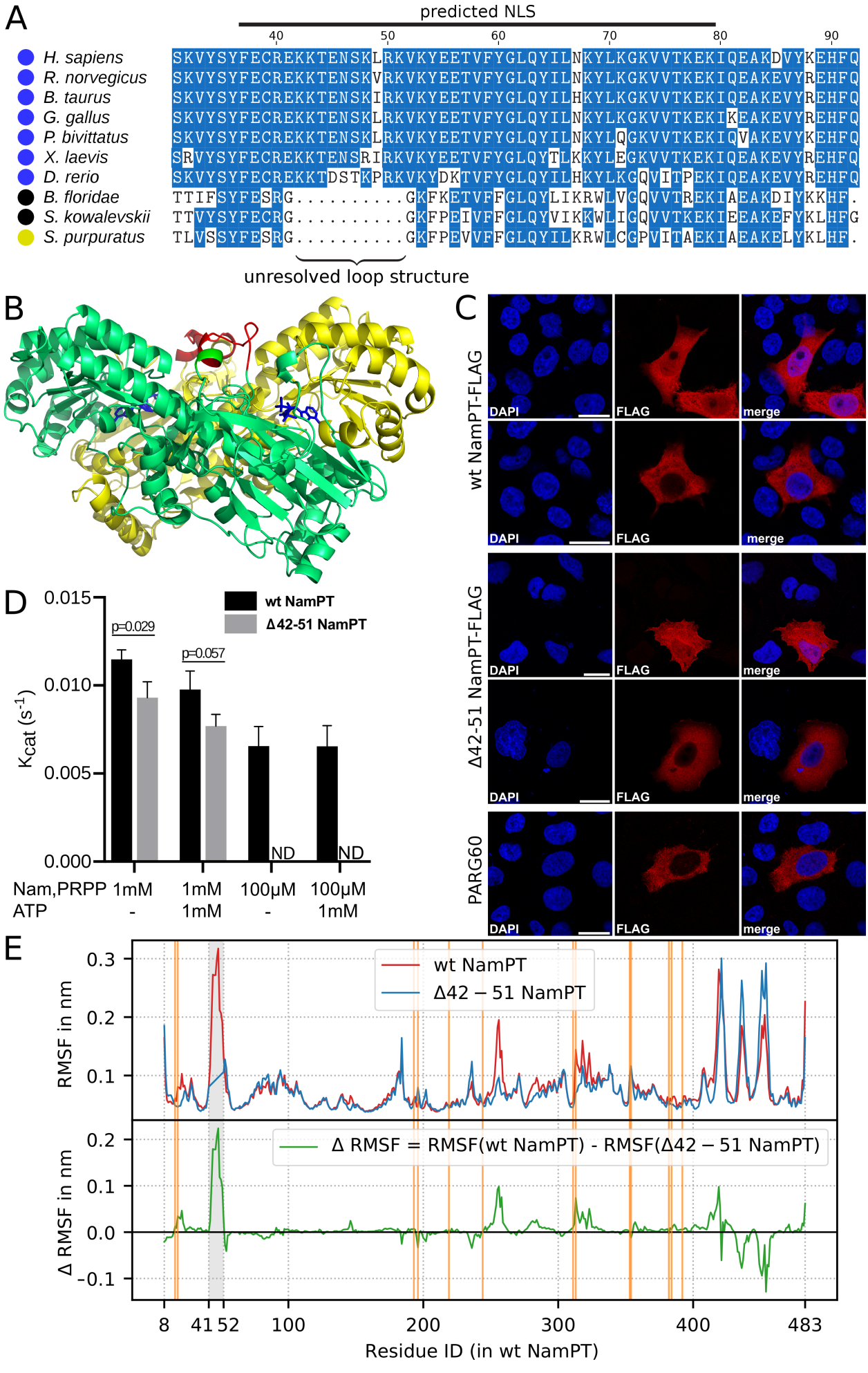

Figure 5: The function of the structurally unresolved loop of NamPT. A) A multiple sequence alignment of NamPT revealed a sequence insertion in the N-terminal region of this enzyme in most

Deuterostomia that possess NamPT and NNMT. The relevant sequence section is shown for selected organisms. A more comprehensive alignment can be found in SI Appendix Figure S2. Coloured circles indicate the enzymes present in the respective species; blue: NamPT and NNMT; black: NamPT, NADA and NNMT; yellow: NamPT and NADA. **B)** The structure visualisation of human NamPT is based on a structure prediction by SWISS-MODEL (74, 75) using the model 2H3D of the human NamPT as template (65). The region corresponding to amino acids 42-51 (shown in red) in the human enzyme is not resolved in any of the currently available crystal structures of NamPT and thus appears to be a flexible loop at the surface of the NamPT dimer. **C)** Confocal laser scan micrographs of HeLaS3 cells expressing C-terminally FLAG-tagged wildtype (wt) and mutant Δ42-51 NamPT lacking the unresolved loop. Both proteins showed a heterogeneous nuclear-cytosolic localisation. Nuclei were stained with DAPI. The C-terminally FLAG-tagged human poly-ADP-ribose glycohydrolase isoform PARG60 was used as a control for exclusive cytosolic localization. (scale bars = 20 µm) **D)** Measurement of NamPT (wildtype and Δ42-51 mutant) enzymatic activity in the presence of 1 mM or 100 µM substrate (Nam and PRPP) with or without 1mM ATP (ND, no detection of the reaction product, NMN). The p-value was calculated using non-parametric one-tailed Mann-Whitney test. The His-tagged proteins were expressed in *E. coli* and purified as described in Methods and Materials (see also SI Appendix Figure S4). **E)** Molecular dynamics simulations were performed for wildtype (red) and Δ42-51 NamPT (blue). Root mean square fluctuations (RMSF) for every residue of chain A are shown (top). The difference RMSF for every residue is shown in the lower panel (green). For better comparison the residue IDs for Δ42-51 NamPT are aligned to accord with the wildtype structure and the average RMSF of residues 42 and 51 displayed in the blue curve between these residues. For the RMSF calculation, the first 100 ns of the simulation are omitted to allow equilibration. In addition, root mean square deviation (RMSD) values between different published structures of human NamPT structures were calculated and presented in SI Appendix Table S4 and Figure S5. The orange lines indicate the position of residues involved in substrate binding, according to Burgos et al. 2009 (35).

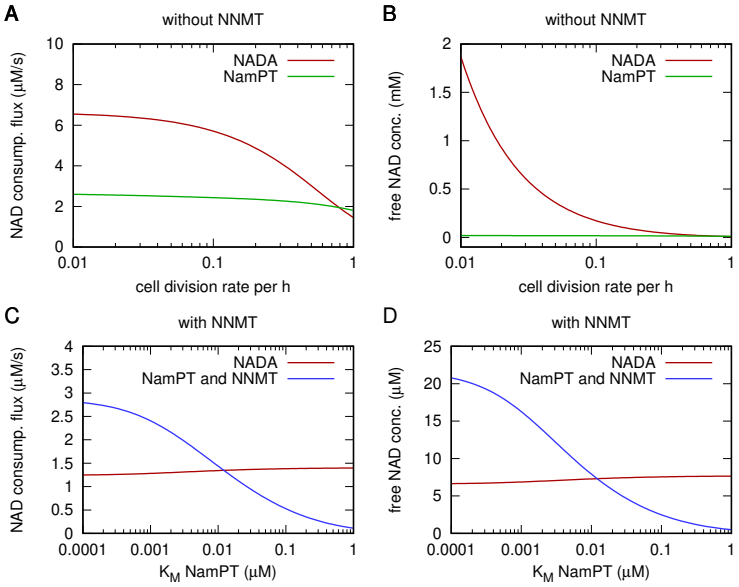

Figure 6: NNMT provides a competitive advantage and makes NADA obsolete in vertebrates. To simulate competition for common resources, a two-compartment model was created (see Methods and Materials and SI Appendix Table S3). In this model one compartment contained NADA, but no NamPT and the other compartment contained NamPT either with or without NNMT, but no NADA. NADA and NamPT were simulated to be present at equal amounts. **A)** In the absence of NNMT, the compartment containing NADA has a higher NAD consumption rate, and **B)** a considerably higher steady state NAD concentration. **C)** In the presence of NNMT, however, both NAD consumption and **D)** NAD concentration are lower in the NADA compartment. This effect is dependent on a high affinity of NamPT for Nam.

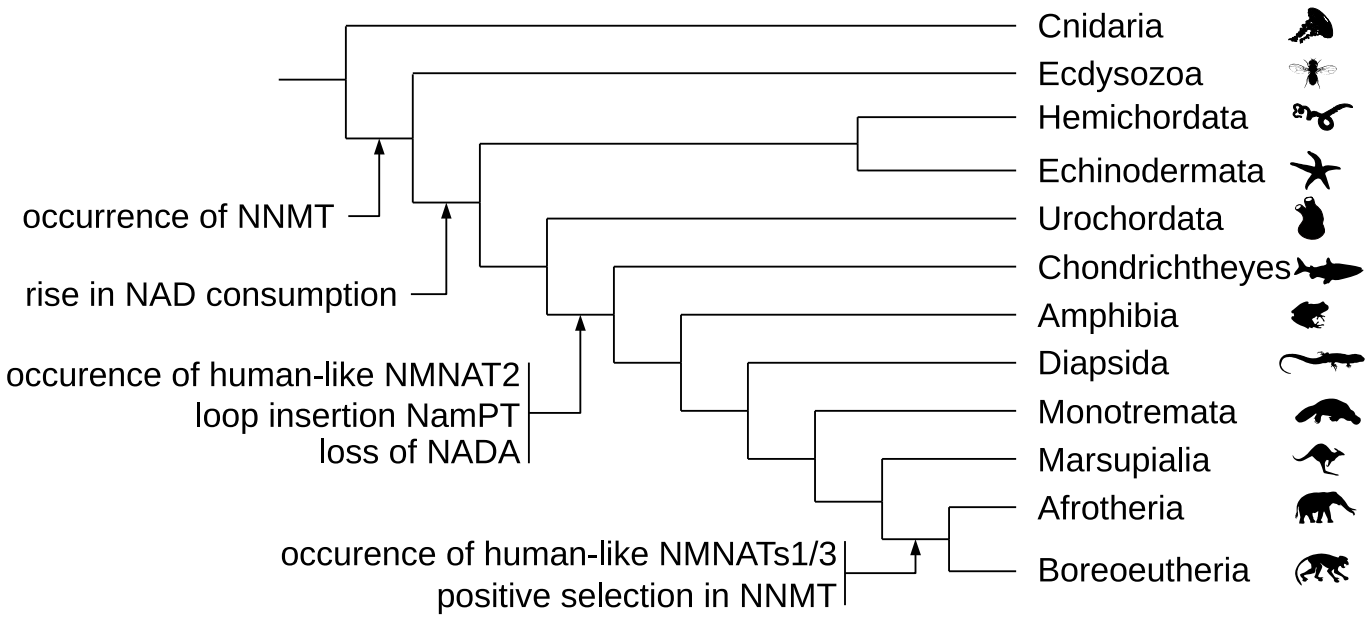

Figure 7: Schematic representation of evolutionary events in the NAD biosynthesis pathway The scheme illustrates major evolutionary events in Metazoa detected in our phylogenetic analyses of NAD metabolism. The time of occurrence of human like NMNAT1 and 3 has been reported previously (61), and identified that human-like NMNAT2 most likely originated in the last common ancestor (LCA) of vertebrates, while human-like NMNAT1/3 can be traced back to the LCA of Placentalia (SI Appendix Figure S9). To test whether the rise of human like NMNAT1/3s was associated with an event of rapid sequence diversification in NNMT we conducted a test of positive selection specific to the branch leading to the LCA of Placentalia using a coding DNA substitution rate ratio model. Indeed, we obtain a strong signature of positive selection for NNMT in the tested branch and can pinpoint residue 171 as being significantly associated with the signature of positive selection (SI Appendix Figures S7 and S8). Specific events in the evolution of NMNATs coincide with those of NamPT or NNMT indicating a co-evolution of functions beyond those identified in the present study. The tree is a schematic representation of selected taxa and is based on information provided by the Tree of life Web Project (76).